Layered Molecule-Based Magnets Formed by Decamethylmetallocenium Cations and Two-Dimensional Bimetallic Complexes [M^{II}Ru^{III}(ox)$_3$]$^-$(M^{II} = Mn, Fe, Co, Cu and Zn; ox = oxalate)

Eugenio Coronado,*,[1] José R. Galán-Mascarós,*,[2] Carlos J. Gómez-García,*
José M. Martínez-Agudo,* Eugenia Martínez-Ferrero,* Joao C. Waerenborgh,†
and Manuel Almeida†

*Instituto de Ciencia Molecular, Universidad de Valencia, Doctor Moliner 50, E-46100 Burjasot, Spain; and †Instituto Tecnológico e Nuclear,
Química, 2686-953 Sacavém, Portugal
E-mail: eugenio.coronado@uv.es

IN DEDICATION TO THE LATE PROFESSOR OLIVIER KAHN FOR HIS PIONEERING CONTRIBUTIONS TO THE FIELD OF MOLECULAR MAGNETISM

A new series of hybrid organometallic-inorganic layered magnets with formula [Z^{III}Cp$_2^*$] [M^{II}Ru^{III}(ox)$_3$] (Z^{III} = Co and Fe; M^{II} = Mn, Fe, Co, Cu, and Zn; ox = oxalate: Cp* = pentamethylcyclopentadienyl) has been prepared. All of these compounds are isostructural to the previously reported [Z^{III}Cp$_2^*$] [$M^{II}M^{III}$(ox)$_3$] (M^{III} = Cr, Fe) series and crystallize in the monoclinic space group C2/m, as found by powder X-ray diffraction analysis. They are novel examples of magnetic materials formed by bimetallic oxalate-based extended layers separated by layers of organometallic cations. The magnetic properties of all these compounds have been investigated (ac and dc magnetic susceptibilities and field dependence of the isothermal magnetization at 2 K). In particular, it has been found that Fe^{II} and Co^{II} derivatives behave as magnets with ordering temperatures of 12.8 and 2.8 K, respectively, while no long-range magnetic ordering has been detected down to 2 K in the Mn^{II} and Cu^{II} derivatives. The magnetic ordering in the Fe^{II} derivatives has been confirmed through Mössbauer spectroscopy. This technique has also made it possible to observe the spin polarization of the paramagnetic [FeCp$_2^*$]$^+$ units caused by the internal magnetic field created by the bimetallic layers in the ordered state. © 2001 Academic Press

Key Words: magnetic multilayer; layered magnet; crystal engineering; magnetic properties; exchange interactions; bimetallic complexes; decamethylferrocenium.

INTRODUCTION

Molecular chemistry provides a versatile basis for the design of novel classes of magnetic materials that can exhibit useful properties or a combination of properties (1). An illustrative example of this concept is provided by the oxalate-bridged bimetallic complexes, which form extended magnetic networks of dimensionalities two (2-D) and three (3-D). These lattices are formed when to an aqueous solution containing the molecular precursors [M^{III}(ox)$_3$]$^{3-}$ (M^{III} = Cr, Fe, Ru) and M^{2+}(aq) (M^{II} = Mn, Fe, Co, Ni, Cu), a bulky cation is added. The insoluble salt so obtained combines the polymeric anion network [$M^{II}M^{III}$(ox)$_3$]$^-$ with a molecular cation that plays the role of template as it controls the connectivity between the two metal complexes and thus the type of crystal structure.

The use of a bulky organic cation of the type [XR_4]$^+$ (X = N, P; R = phenyl, n-propyl, n-butyl, etc.) stabilizes the formation of a 2-D network wherein the M^{III} and M^{II} ions alternate at the corners of a hexagonal layer (Fig. 1a). These layers are interleaved by organic cations that determine the interlayer separation and the packing of the layers (2). All these compounds behave as magnets with critical temperatures, T_c, ranging from 5 to 44 K (3–6). The use of a chiral cation such as [Z^{II}(bpy)$_3$]$^{2+}$ (Z^{II} = Fe, Co, Ni, Ru, Zn) has led to the formation of a chiral 3-D structure (7). These compounds have also shown to behave as magnets but with lower critical temperatures (8).

Insertion of other cations has recently been explored with the idea of adding complexity to the two-network magnet, or even to obtain multifunctional materials in which magnetism is combined with a second physical property (9). Thus, the use of paramagnetic cations such as decamethylferrocenium, [FeCp$_2^*$]$^+$ (Fig. 1b) has provided examples of chemically constructed magnetic multilayers in which ferromagnetic M^{II}Cr^{III} (or ferrimagnetic M^{II}Fe^{III}) layers alternate with layers of paramagnetic cations (10, 11). With the
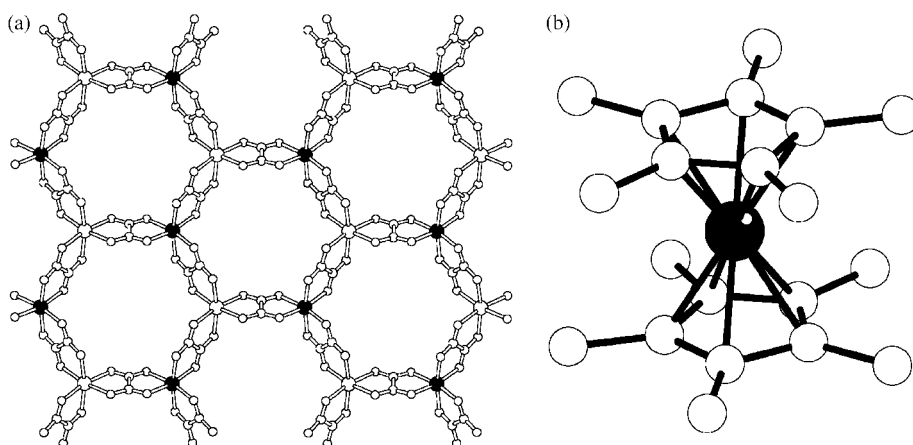
FIG. 1. (a) View of the structure of the $[M^{II}M^{III}(ox)_3]^-$ 2D hexagonal honey-comb layer; (b) view of the structure of the decamethylferrocenium cation, $[FeCp_2^*]^+$ (hydrogen atoms have been omitted for clarity).

aim of conferring a novel property on the magnetic material we have inserted the π-electron donor molecule bis(ethylenedithio)tetrathiafulvalene (BEDT-TTF) in between the $Mn^{II}Cr^{III}$ layers. Interestingly, a coexistence of ferromagnetism and metallic conductivity has been observed in this case (12). In the same context, it has been possible to insert complexes exhibiting spin crossover (13) or organic dyes that give rise to nonlinear optical properties (14).

In the present paper we will focus on the novel hybrid magnets obtained by combining the complexes $[Ru^{III}(ox)_3]^{3-}$ and $M^{2+}(aq)$ with the organometallic monocations $[FeCp_2^*]^+$ and $[CoCp_2^*]^+$. The only work devoted to the magnetic properties of oxalate-bridged layered magnets based upon Ru^{III} was published by Kahn and coworkers in 1998 (15). When the molecular magnetism community was still intrigued by the novel and, in some cases, surprising properties of the $[M^{II}Cr^{III}]$ and $[M^{II}Fe^{III}]$ oxalate series. Olivier enlarged the opportunities provided by these polymeric complexes by preparing a completely new series based on the magnetically interesting Ru^{III} ion. In that paper three novel 2-D compounds of formula $(NBu_4)[M^{II}Ru^{III}(ox)_3]$ (M = Mn, Fe, and Cu) were reported. The motivation of the work was to explore how the introduction of Ru^{III} (instead of Cr^{III} or Fe^{III}) into the bimetallic network affected the magnetic properties of the material. The most surprising result concerned the nature of the Ru^{III} – M^{II} interaction that was proposed to be antiferromagnetic for M = Fe and Cu and ferromagnetic for M = Mn.

EXPERIMENTAL

Synthesis

The precursor $K_3[Ru(ox)_3] \cdot 4.5H_2O$ was prepared as described in literature (15), while all other reagents were used as purchased.

$[CoCp_2^*][Mn^{II}Ru^{III}(ox)_3]$ **(1)**. $[CoCp_2^*][PF_6]$ (0.12 g, 0.26 mmol) dissolved in dimethylformamide (DMF, 5 mL) was added slowly to an aqueous solution (6 mL) of $K_3[Ru(ox)_3] \cdot 4.5H_2O$ (0.15 g, 0.26 mmol) and $MnCl_2 \cdot 4H_2O$ (0.11 g, 0.52 mmol). After several minutes a green precipitate appeared that was filtered in vacuo, washed with water and DMF, and dried at room temperature.

$[CoCp_2^*][Fe^{II}Ru^{III}(ox)_3]$ **(2)**. This compound was synthesized as a green precipitate as described above for **1** but with $FeSO_4 \cdot 7H_2O$ (0.09 g, 0.34 mmol) instead of $MnCl_2 \cdot 4H_2O$ and the amount of $[CoCp_2^*][PF_6]$ was increased (0.18 g, 0.38 mmol, in 5 mL of DMF).

$[CoCp_2^*][Cu^{II}Ru^{III}(ox)_3]$ **(3)**. This compound was synthesized as a green precipitate as described above for **1** but with $Cu(NO_3)_2 \cdot 3H_2O$ (0.1 g, 0.42 mmol) instead of $MnCl_2 \cdot 4H_2O$ and the amount of $[CoCp_2^*][PF_6]$ was increased (0.2 g, 0.42 mmol, in 5 mL of DMF).

$[CoCp_2^*][Co^{II}Ru^{III}(ox)_3]$ **(4)**. This compound was synthesized as a green precipitate as described above for **1** but with $Co(NO_3)_2 \cdot 6H_2O$ (0.15 g, 0.52 mmol) instead of $MnCl_2 \cdot 4H_2O$.

$[CoCp_2^*][Zn^{II}Ru^{III}(ox)_3]$ **(5)**. This compound was synthesized by adding successively an aqueous solution of $Zn(NO_3)_2 \cdot 6H_2O$ (0.2 g, 0.65 mmol, 1 mL) and a solution of $[CoCp_2^*][PF_6]$ (0.15 g, 0.3 mmol, in 2.5 mL of DMF) to an aqueous solution of $K_3[Ru(ox)_3] \cdot 4.5 H_2O$ (0.14 g, 0.25 mmol, 1.5 mL). After stirring for 30 min. a green precipitate appeared. The solution was filtered in vacuo, washed with water and DMF, and dried at room temperature.

$[FeCp_2^*][Mn^{II}Ru^{III}(ox)_3]$ **(6)**. $[FeCp_2^*][BF_4]$ (0.15 g, 0.35 mmol) dissolved in warm distilled water (25 mL) was

added slowly to an aqueous solution (3 mL) of $K_3[Ru(ox)_3] \cdot 4.5H_2O$ (0.2 g, 0.35 mmol) and $MnCl_2 \cdot 4H_2O$ (0.2 g, 1.05 mmol). After stirring for 1 h, the resulting solution was filtered in vacuo, obtaining a green precipitate that was washed with water and dried at room temperature.

$[FeCp_2^*][Fe^{II}Ru^{III}(ox)_3]$ (**7**). This compound was synthesized as a green precipitate as described above for **6** but with $FeSO_4 \cdot 7H_2O$ (0.29 g, 1.05 mmol) instead of $MnCl_2 \cdot 4H_2O$.

$[FeCp_2^*][Cu^{II}Ru^{III}(ox)_3]$ (**8**). This compound was synthesized as a green precipitate as described above for **6** but with $Cu(NO_3)_2 \cdot 3H_2O$ (0.15 g, 0.62 mmol) instead of $MnCl_2 \cdot 4H_2O$, and the proportion of $[FeCp_2^*][BF_4]$ was increased (0.24 g, 0.58 mmol, in 39 mL of H_2O).

$[FeCp_2^*][Co^{II}Ru^{III}(ox)_3]$ (**9**). This compound was synthesized as a green precipitate as described above for **6** but with $Co(NO_3)_2 \cdot 6H_2O$ (0.21 g, 0.7 mmol) instead of $MnCl_2 \cdot 4H_2O$.

$[FeCp_2^*][Zn^{II}Ru^{III}(ox)_3]$ (**10**). This compound was synthesized by adding successively an aqueous solution (6 mL) of $Zn(NO_3)_2 \cdot 6H_2O$ (0.58 g, 1.9 mmol) and another solution (37.5 mL) of $[FeCp_2^*][BF_4]$ (0.25 g, 0.6 mmol) dissolved in warm distilled water to a solution of $K_3[Ru(ox)_3 \cdot 4.5H_2O$ (0.35 g, 0.6 mmol) dissolved in H_2O (6 mL). After stirring for 15 min., a green precipitate appeared. The solution was filtered in vacuo, washed with water, and dried at room temperature.

X-Ray Diffraction

X-ray powder profiles were collected using a Siemens D-500 X-ray diffractometer ($CuK\alpha$ radiation). Samples were ground and mounted on a flat sample plate. Typically, profiles were collected as step scans over a 12-h period in the $2° < 2\theta < 60°$ range with a step size of $0.02°$. The powder patterns reported in this work were indexed and refined successfully in a monoclinic space group.

Magnetic Measurements

Variable-temperature dc susceptibility measurements were carried out on polycrystalline samples in the temperature range 2–300 K at a magnetic field of 1 kOe. The susceptibility data were corrected for the diamagnetic contributions calculated from Pascal's constant tables. Variable-temperature ac susceptibility measurements were carried out in the temperature range 2–20 K, with an alternating applied field of 3.95 Oe at different frequencies (1–100 Hz). Hysteresis loops were measured between 50 and − 50 kOe. All of these measurements were carried out with a magnetometer (Quantum Design MPMS-XL) equipped with a SQUID sensor.

Mössbauer Data

^{57}Fe Mössbauer measurements were recorded in transmission mode using a conventional constant acceleration spectrometer and a 25-mCi ^{57}Co source in the Rh matrix. The velocity scale was calibrated using an α-Fe foil at room temperature. Isomer shift values are given relative to this standard. Spectra were collected with the absorbers between 296 and 5 K. Low-temperature measurements were obtained using a flow cryostat (temperature stability $\pm$ 0.5 K). The spectra were fitted to Lorentzian lines using a nonlinear least-squares fitting method.

RESULTS AND DISCUSSION

Synthesis and Structure

A total of 10 compounds divided into two different series, namely the decamethylcobaltocenium series $[CoCp_2^*][M^{II}Ru^{III}(ox)_3]$ (M = Mn, Fe, Co, Cu, and Zn) and the corresponding decamethylferrocenium series $[FeCp_2^*][M^{II}Ru^{III}(ox)_3]$, were synthesized by the addition of a solution of the organometallic cation (in water, or DMF in the case of the decamethylcobaltocenium) to an aqueous solution of the *tris*-oxalate ruthenate complex with an excess of the divalent metal.

The compounds were obtained as green microcrystals and were all isostructural as demonstrated by X-ray powder diffraction (Fig. 2). In fact, the diffraction patterns were found to be very close to those of the analogous $M^{II}Cr^{III}$ and $M^{II}Fe^{III}$ derivatives, whose crystal structure has been previously solved (10). The reflections were indexed and the unit cell parameters were refined in the monoclinic
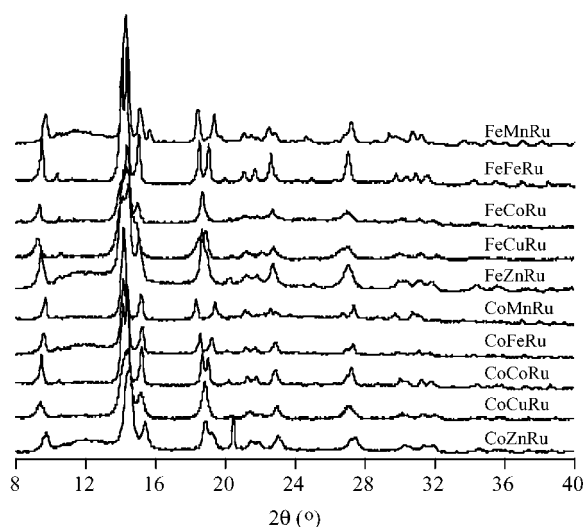

FIG. 2. X-ray powder patterns for the series of compounds $[M^{III}Cp_2^*])[M^{II}Ru^{III}(ox)_3]$ (M^{III} = Co, Fe; M^{II} = Mn; Fe, Co, Cu, Zn).

TABLE 1
Unit Cell Parameters for the Series $[Z^{III}Cp_2^*]$ $[M^{II}Ru^{III}(ox)_3]$ Obtained by Powder X-Ray Diffraction

$Z^{III}M^{II}Ru^{III}$	a (Å)	b (Å)	c (Å)^a	β (o)	V (Å^3)
FeMnRu	9.004(16)	17·106(16)	9.189(7)	93.56(4)	1412.7(3)
FeFeRu	8.981(18)	17.06(3)	9.228(17)	93.63(12)	1411.4(6)
FeCoRu	9.019(9)	17.088(16)	9.202(8)	93.38(5)	1415.7(3)
FeCuRu	9.03(3)	17.14(8)	9.18(4)	93.64(19)	1417.2(11)
FeZnRu	8.993(17)	17.12(3)	9.183(17)	93.56(10)	1410.9(5)
CoMnRu	9.059(11)	17.204(14)	9.173(12)	94.13(7)	1425.9(4)
CoFeRu	8.974(13)	17.088(23)	9.224(11)	95.57(7)	1411.8(4)
CoCoRu	9.032(13)	17.216(20)	9.286(15)	93.72(9)	1441.0(5)
CoCuRu	8.985(15)	17.082(25)	9.181(10)	93.46(7)	1406.5(5)
CoZnRu	9.041(11)	17.119(19)	9.218(14)	93.33(11)	1424.2(5)

^{a} This parameter (c) corresponds to the interlayer separation (d).

space group $C2/m$. Unit cell parameters are given in Table 1. These results indicate that these new series of compounds are examples of 2-D bimetallic layers. As in the $M^{II}Cr^{III}$ and $M^{II}Fe^{III}$ derivatives, the organometallic cations are located between the anionic layers and impose an eclipsed staking of the layers (Fig. 3). In this respect it is important to note that these structural features are in sharp contrast to those found in the corresponding $[NBu_4]^+$ derivatives, which are less crystalline and very often exhibit a disorder in the stacking of the layers. Such a difference may significantly affect the magnetic properties.

Magnetic Properties

In this section we will treat first the $[CoCp_2^*]^+$ salts in which the magnetic bimetallic layers alternate with layers of

this diamagnetic cation, and then the $[FeCp_2^*]^+$ salts in which the magnetic bimetallic layers alternate with layers of this paramagnetic $S = \frac{1}{2}$ species.

Decamethylcobaltocenium Salts

Derivatives with $M^{II} =$ Mn, Fe, Co, Cu, and Zn have been studied. Relevant magnetic parameters are given in Table 2.

[ZnRu]. This compound shows a paramagnetic behavior in the whole temperature range (down to 2 K), in full agreement with the magnetic insulation of the paramagnetic Ru^{III} ion in the bimetallic net, as each Ru^{III} is surrounded by three diamagnetic Zn^{II} ions. However, the Curie law is not obeyed. Instead, down to 15 K the data can be fitted to a Curie–Weiss law, with a negative Weiss constant, $\theta = -5.3$ K, and a Curie constant of 0.4 emu.K.mol^{-1}. On the other hand, a sharp decrease of the χT product is observed below 15 K, which changes from 0.32 emu.K.mol^{-1} at 15 K to a value of 0.22 emu.K.mol^{-1} at 2 K (Fig. 4). This behavior is consistent with an incomplete quenching of the orbital contribution to the magnetic moment, in full agreement with the orbitally degenerate ground state of Ru^{III}. In the magnetically condensed compounds, this feature may prevent the correlation of the sign of θ with the sign of the Ru^{III}–M^{II} interaction. For example, a negative θ value (or a minimum in the χT vs T plot) will not necessarily involve an antiferromagnetic exchange interaction. Inspection of the saturation magnetization in the low-temperature M vs H plot will be then required to get additional information on this point. In order to study the magnetization of the Ru^{III} ion, we have measured the [ZnRu] compound. As we can see, the isothermal magnetization at 2 K shows a continuous increase when the field is
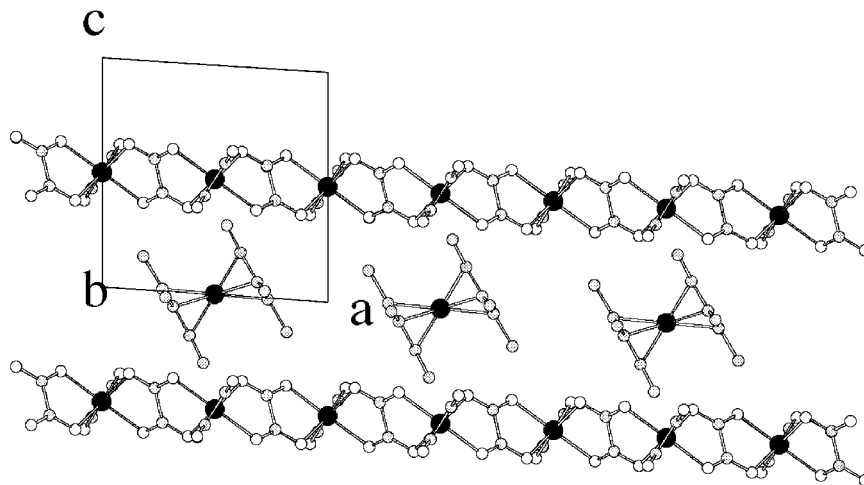

FIG. 3. View of the structure of the $[Fe^{III}Cp_2^*][Mn^{II}Cr^{III}(ox)_3]$ compound, showing the alternating $[Fe^{III}Cp_2^*]^+$ and $[Mn^{II}Cr^{III}(ox)_3]^-$ layers.

TABLE 2
Magnetic Parameters for the Series $[CoCp_2^*]$ $[M^{II}Ru^{III}(ox)_3]$

$M^{II}Ru^{III}$	C (emu K mol^{-1})	C_{SO} (emu K mol^{-1})	θ (K)	T_c (K)	$M(\mu_B)$	$M_r(\mu_B)$	H_{coer} (kOe)
MnRu	4.5	4.37	-0.4	<2	5.0	0.0	0.00
FeRu	3.6	3.76	10.1	12.8	2.8	2.0	3.20
CoRu	4.3	3.40	-22.3	2.8	2.8	0.0	0.00
CuRu	0.8	0.80	-0.1	<2	1.5	0.0	0.00
ZnRu	0.4	0.36	-5.3	—	0.6	—	—

Note. Parameters are experimental Curie constant C, calculated spin-only Curie constnat (C_{SO}), Weiss constant (θ), critical temperature (T_c), magnetization at 50 kOe and 2 K (M), remnant magnetization at 2 K (M_r) and coercive field at 2 K (H_{coer}).

increased, and reaches a value close to 0.6 μ_B at 50 kOe, although it does not saturate (inset of Fig. 4).

[*MnRu*] *and* [*CuRu*]. These two compounds also stay paramagnetic down to 2 K. The χT vs T curves are shown in Figs. 5 and 6. The room temperature values roughly correspond to what is expected for isolated magnetic centers, with local spins $S_{Ru} = \frac{1}{2}$, $S_{Mn} = \frac{5}{2}$, and $S_{Cu} = \frac{1}{2}$. In [MnRu] the χT product stays almost constant down to 30 K and shows a steady increase upon further cooling. Such a behavior is consistent with a weak ferromagnetic Ru^{III}–Mn^{II} interaction. The field dependence of the magnetization at 2 K confirms this conclusion. It shows a rapid increase of M in the low field and a tendency to saturate at higher field with a value of 5.0 μ_B at 50 kOe. This value is lower than that expected for a parallel alignment of the two interacting spins (on the order of 6 μ_B). Still, the contribution of the Ru^{III} ion can be smaller, as shown in Fig. 4, due to its anisotropy.
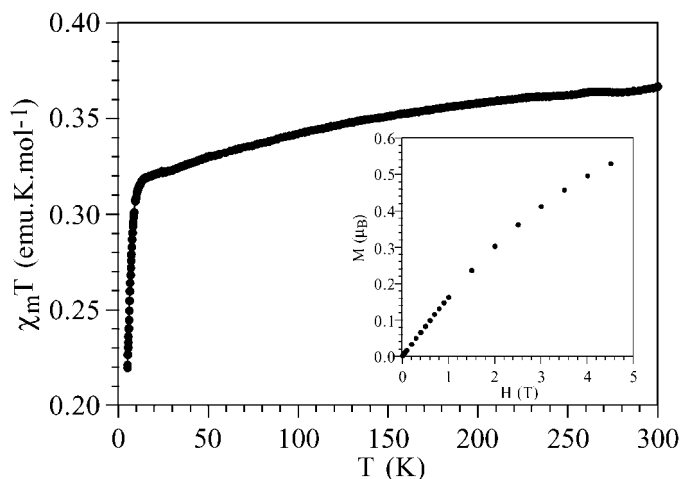

FIG. 5. Plot of the $\chi_m T$ product vs T and of the magnetization vs applied field at 2 K (inset), for $[CoCp_2^*][MnRu(ox)_3]$ (**1**).
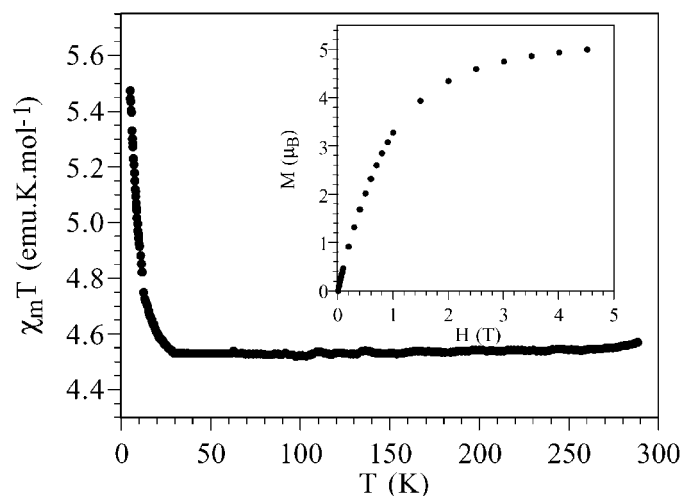
At first sight, similar magnetic features are observed in [CuRu]. A closer look of the χT vs T plot indicates however a decrease from a value of 0.87 emu.K.mol^{-1} at room temperature to a minimum of 0.79 emu.K.mol^{-1} at approx. 80 K, followed by an increase at lower temperatures. In principle, such a behavior may indicate a ferrimagnetic behavior, i.e., an antiferromagnetic coupling between the two noncompensated magnetic moments. Since both Ru and Cu carry a spin $\frac{1}{2}$, different local Landé factors are required to produce a ferrimagnetic behavior. However, the small decrease in χT should require very different magnetic moments, a situation that seems to be unrealistic in the present case. An alternative explanation requires then a ferromagnetic Ru^{III}–Cu^{II} interaction. Under such an assumption the slight decrease in χT could be merely a result of the single-ion behavior of Ru^{III} (*vide supra*). Such an explanation is more realistic, and furthermore is in agreement with the symmetry rules governing the nature of the exchange interaction. In fact, this interaction involves two orthogonal magnetic orbitals as the unpaired electron of Ru^{III} is located at t_{2g}-type orbitals, while for Cu^{II} it is located at the $d_{x^2-y^2}$ orbital. The field dependence of the magnetization at low temperatures (2 K) also supports a ferromagnetic coupling. Thus, a sharp increase of M in low field is observed followed by a progressive saturation toward a value of 1.5 μ_B at 50 kOe, which is very close to what is expected for a parallel alignment of Ru^{III} and Cu^{II} magnetic moments.

[*FeRu*] *and* [*CoRu*]. The temperature dependence of the dc and ac magnetic susceptibilities and the field dependence of the magnetization suggest that these two compounds exhibit long-range magnetic ordering at low temperatures.
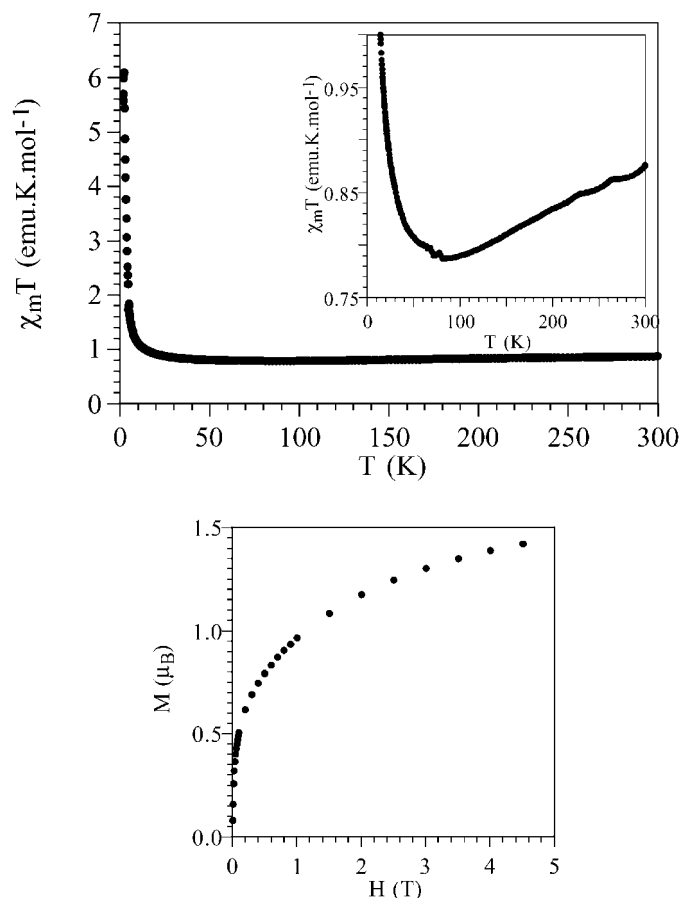

FIG. 4. Plot of the $\chi_m T$ product vs T and of the magnetization vs applied field at 2 K (inset), for $[CoCp_2^*][ZnRu(ox)_3]$ (**5**).

FIG. 6. Plot of the $\chi_m T$ product vs T (top) and of the magnetization vs applied field at 2 K (bottom) for $[CoCp_2^*][CuRu(ox)_3]$ (**4**).

FIG. 7. (top) Plot of the $\chi_m T$ product vs T and of the ac susceptibility measurements (inset) for $[CoCp_2^*][FeRu(ox)_3]$ (**2**); (bottom) hysteresis loop at 2 K.

Thus, in [FeRu] an abrupt increase in both χ and χT at temperatures below 20 K is observed (Fig. 7), which indicates that the magnetic ordering is nearby this temperature. To determine more precisely the critical temperature, T_c, we have performed ac magnetic susceptibility measurements. Typically, in a magnet containing net magnetic moments in the ordered state (ferromagnet, ferrimagnet, or canted antiferromagnet, for example) a maximum in the in-phase signal (χ') near T_c and an out-of-phase signal (χ'') that starts to appear at temperatures just below T_c are observed. In [FeRu] the maximum in χ' is clearly observed at approx. 12 K, together with the corresponding χ'' signal (inset of Fig. 7). From these data the estimated T_c value is 12.8 K. In this case T_c is determined with a certain uncertainty (± 0.2 K) due to the slight dependence of the ac magnetic responses with the frequency of the oscillating magnetic field. This weak frequency dependence is not unusual in the oxalate magnets containing Fe(II). Similar behaviors have already been observed in the related 2D and 3D bimetallic [FeCr] phases and have been attributed to the presence of small amounts of Fe^{III} ions in the bimetallic network, which
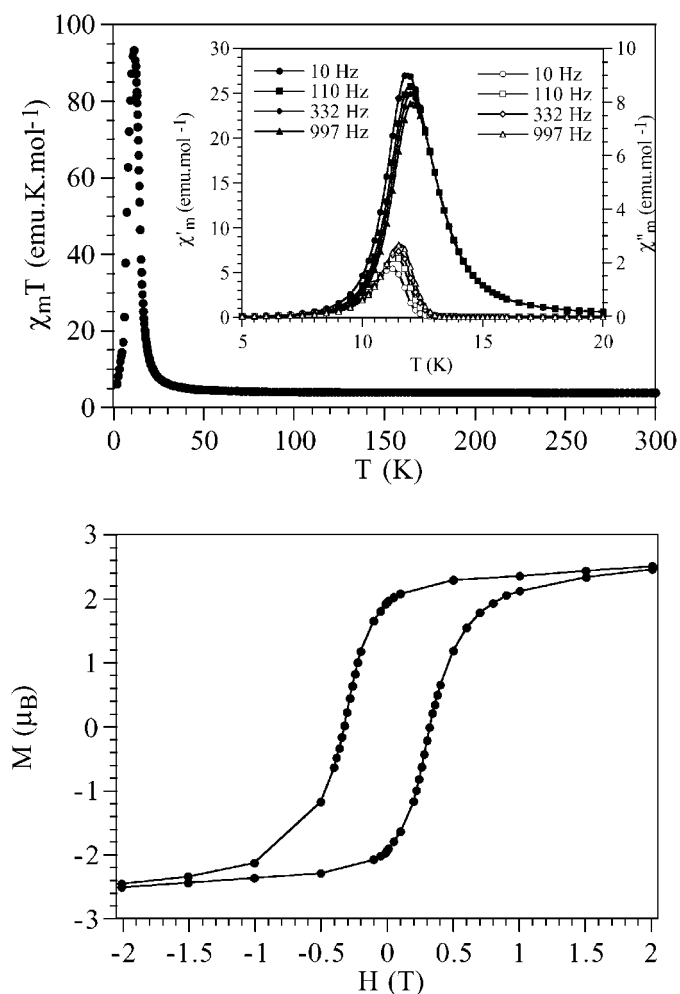
introduces some magnetic disorder in the lattice as a result of the presence of antiferromagnetic Fe^{III}–Fe^{II} interactions competing with Cr^{III}–Fe^{II} interactions (8,10b). Finally, a controversial point deals with the nature (ferromagnetic or antiferromagnetic) of the Ru^{III}–Fe^{II} interaction. Inspection of the field dependence of the isothermal magnetization performed at 2 K suggests that the magnetic ordering is ferrimagnetic. In fact, one observes a rapid raise of the magnetization with H in low fields (up to 10 kOe). Above this field M increases much smoother in a linear way from a value of 2.1 μ_B at 10 kOe to a value of 2.8 μ_B at 50 kOe. This last value is close to the saturation value expected for an antiparallel alignment of the two interacting spin sublattices ($S_{Ru^{III}} = \frac{1}{2}$, $S_{Fe^{II}} = 2$), which is about 3 μ_B, and supports an antiferromagnetic Ru^{III}–Fe^{II} interaction. However, the possibility of a ferromagnetic Ru^{III}–Fe^{II} interaction cannot be ruled out because in these kinds of layered magnets a spin

TABLE 3
Magnetic Parameters for the Series [CoCp$_2^*$] [$M^{III}Cr^{III}(ox)_3$]

$M^{II}Cr^{III}$	T_c (K)	M (μ_B)	M_r (μ_B)	H_{coer} (kOe)
MnCr	5.1	7.0	0.3	0.04
FeCr	12.7	4.6	3.5	1.94
CoCr	8.2	5.0	1.3	0.25
CuCr	6.7	3.6	1.7	0.20

Note. Parameters are critical temperature (T_c), magnetization at 50 kOe and 2 K (M), remnant magnetization at 2 K (M_r) and coercive field at 2 K (H_{coer}).

canting is also present, which can lead to a significant reduction in the magnetization values. Such an effect is expected to be particularly pronounced for the more anisotropic ions (Fe^{II} and Co^{II}). For example, in the [CoCp$_2^*$]$^+$ salt of the [FeCr] ferromagnet the magnetization at 50 kOe was on the order of 4.6 μ_B (Table 3), whereas the expected saturation value for a parallel alignment of the magnetic moments should be close to 7 μ_B. Since for the isotropic Cr^{III} ion the saturation magnetization is close to 3 μ_B, Fe^{II} is expected to contribute to the total magnetization with 1.6 μ_B. In the present case, [RuFe], this kind of argument should lead to magnetization values on the order of 2.6 μ_B, in perfect agreement with the experimental value. The ferromagnetic interaction is also supported by the calculated Weiss constant, which has been found to be clearly positive in the present case ($\theta = 10.1$ K), despite the negative contribution coming from the Ru^{III}. Finally, a magnetic hysteresis loop is also observed at low temperatures with a large coercive field of 3.2 kOe and a remnant field of 2 μ_B at 2 K (Fig. 7). These features are typical of hard magnets.

In the [CoRu] derivative the magnetic properties also show evidence of long-range ordering. Thus, χT diverges at very low temperatures and the ac susceptibilities present a maximum in χ' at 2.6 K and a χ'' signal below 2.8 K, which defines T_c (Fig. 8). In contrast to the previous case, these signals are frequency independent, as expected for a magnet. The field dependence of the isothermal magnetization at 2 K shows a sharp rise at low field and tends to a value of 2.8 μ_B at 50 kOe. Using the argument similar to that developed in the previous case, one can infer that the Ru^{III}–Co^{II} interaction is also ferromagnetic. Thus, although it is difficult to know the magnetization of the Co(II) sublattice, due to the orbitally degenerate ground state of this ion ($^4T_2$ in octahedral sites), a rough estimate can be done from the saturation magnetization of the analogous [CoCr] derivative (Table 3). In this ferromagnet this value is equal to 5 μ_B and since the Cr(III) contribution is equal to 3 μ_B, one can estimate that the contribution of the Co(II) sublattice is on the order of 2 μ_B. The magnetization value observed in
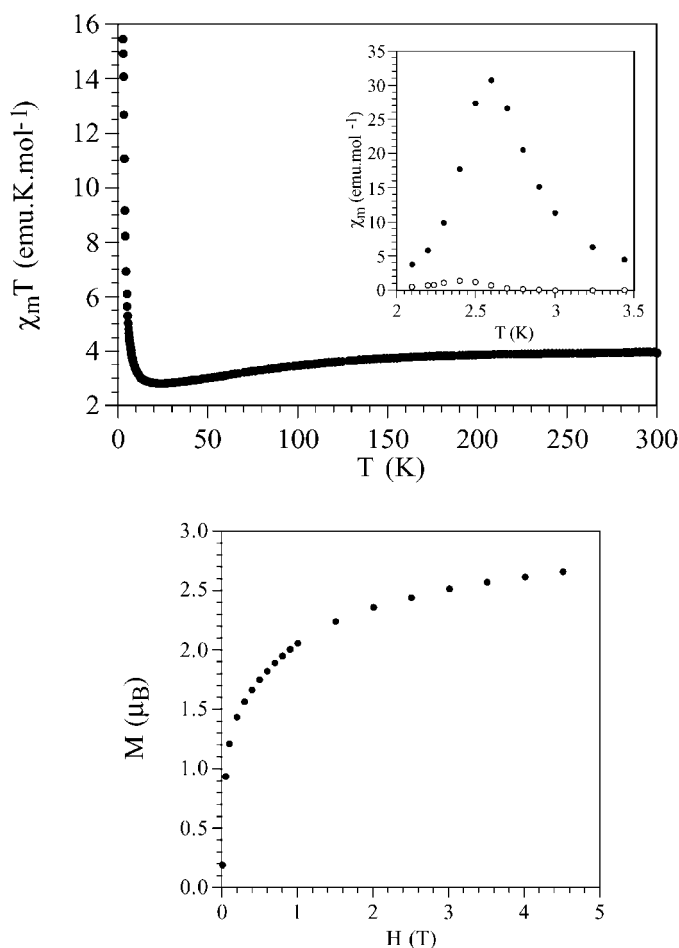
FIG. 8. (top) Plot of the $\chi_m T$ product vs T and of the ac susceptibility measurements (inset) for [CoCp$_2^*$][CoRu(ox)$_3$] (**3**); (bottom) plot of the magnetization vs applied field at 2 K.

the [CoRu] compound (2.8 μ_B) is then in full agreement with the sum of the two magnetic sublattices. Note that a pronounced minimum in χT is observed at approx. 20 K, which may suggest the reverse conclusion (Fig. 8). Once again it is useful to remember that the presence of such a minimum is not always the signature of an antiferromagnetic coupling between uncompensated magnetic moments. This observation is only true when we are dealing with orbitally quenched magnetic ions, and the [CoRu] compound is not the case as in distorted octahedral sites both ions have orbitally degenerate ground states. Finally, it is interesting to emphasize the lack of hysteresis in the magnetization measurements, which makes it possible to refer to the [CoRu] compound as a very soft ferromagnet. This is a somewhat surprising result as the coercivity of a magnet often depends on the magnetic anisotropy of the interacting spin carriers, and both Ru^{III} and Co^{II} are very anisotropic ions.
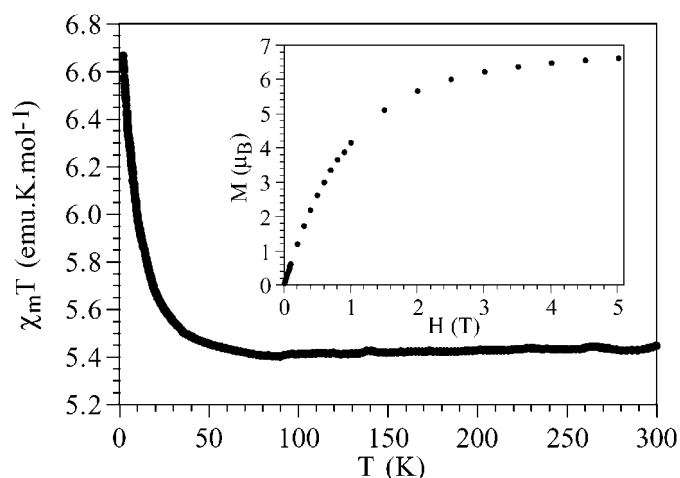
FIG. 9. Plot of the $\chi_m T$ product vs T and of the magnetization vs applied field at 2 K (inset) for $[FeCp_2^*][MnRu(ox)_3]$ (6).

Decamethylferrocenium Salts

When the diamagnetic $[CoCp_2^*]^+$ ion is substituted by the paramagnetic $[FeCp_2^*]^+$ ion we end up with a layered material in which the two kinds of magnetic monolayers alternate in the structure. As in the previous series, the derivatives with $M^{II} = $ Mn, Fe, Co, Cu, and Zn have been prepared and magnetically characterized (Figs. 9–12). We observe that, in general, the magnetic properties of all these compounds are similar to those observed in the $[CoCp_2^*]^+$ series, as demonstrated by the relevant magnetic parameters (critical temperatures and coercive fields) given in Table 4. The only noticeable difference has been seen in the [FeRu] hybrid and refers to the frequency dependence of the ac signals and to the hysteretic behavior. In contrast to the $[CoCp_2^*]^+$ salt, in the $[FeCp_2^*]^+$ salt the ac signals are practically frequency independent (Fig. 10). On the other hand a reduction of the coercive field has been observed (from 3.2 and 2.2 kOe). The first feature may indicate that the amount of disorder in the bimetallic layer is smaller when $[CoCp_2^*]^+$ is substituted by $[FeCp_2^*]^+$. The reduction in the coercive field follows the general trend already pointed out in the [FeCr] derivatives and should be attributed to the presence of the paramagnetic complex, as the structural features of the two series do not change.

All these results indicate that the two magnetic sublattices essentially behave independently, with the magnetic ordering being mainly controlled by the bimetallic oxalate sublattice.

Mössbauer Spectroscopy

Mössbauer spectra of $[CoCp_2^*][FeRu(ox)_3]$ taken between 297 and 14 K (Fig. 13) show a quadrupole doublet

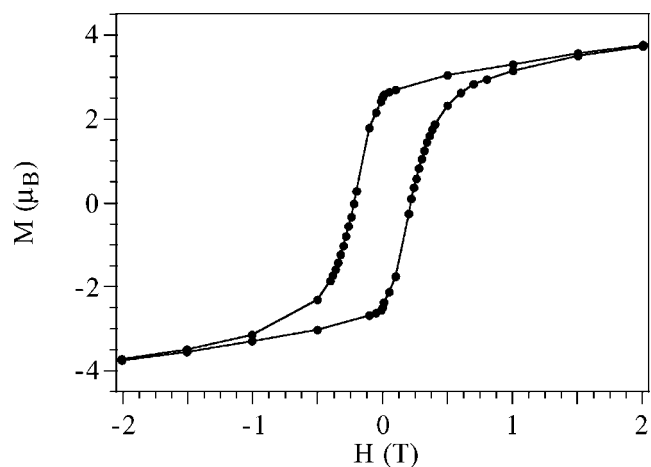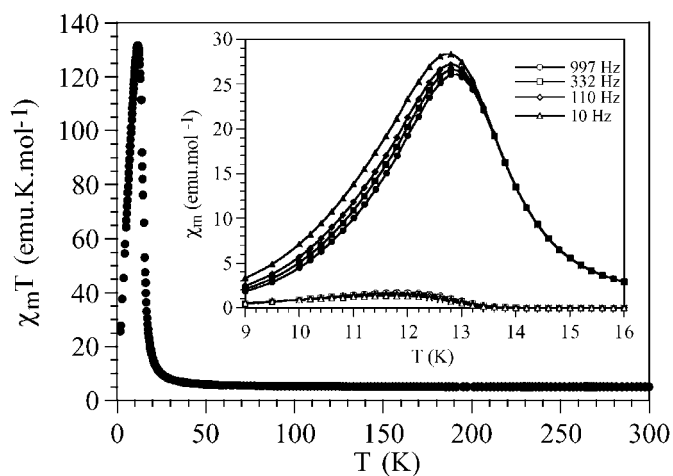**FIG. 10.** (top) Plot of the $\chi_m T$ product vs T and of the ac susceptibility measurements (inset) for $[FeCp_2^*][FeRu(ox)_3]$ (7); (bottom) hysteresis loop at 2 K.

with estimated isomer shift, δ, and quadrupole splitting, Δ (Table 5), similar to those observed for Fe^{II} in the $[FeCr(ox)_3]^-$ complex of other compounds such as $(NBu_4)[FeCr(ox)_3]$ (16), or $[CoCp_2^*][FeCr(ox)_3]$ or $[FeCp_2^*][FeCr(ox)_3]$ (10b).

Below 14 K, in agreement with magnetic measurements, long-range magnetic ordering of the Fe^{II} is established. The Mössbauer spectra (Fig. 13) could not be fitted assuming a simple magnetic sextet. This implies that the quadrupole hyperfine interaction cannot be treated as a perturbation of the magnetic hyperfine interaction. The position and relative intensities of the absorption lines of the magnetically ordered Fe atoms were therefore calculated by solving the complete Hamiltonians for the hyperfine interactions in both the excited and ground nuclear states of the ^{57}Fe nuclei, following the procedure described by Ruebenbauer and Birchall (17).

The best fit of the spectra was obtained assuming that the angle between the magnetic hyperfine field, B_{hf}, and the

main axis of the electric field gradient, V_{zz}, is $\theta = 90°$ and between B_{hf} and V_{xx} is $\phi = 0°$. As in the case of $(NBu_4)[FeCr(ox)_3]$ (16) and $Fe(ox) \cdot 2H_2O$ (18), B_{hf} is perpendicular to the main axis of the electric field gradient and parallel to the shortest axis. The final values obtained for the fitted parameters, δ, B_{hf}, the asymmetry parameter η, and $\Delta' = eQV_{zz}/2$ (18) are given in Table 5, δ and Δ' are similar to those reported for $(NBu_4)[FeCr(ox)_3]$ and $Fe(ox) \cdot 2H_2O$. The B_{hf} value is consistent with high-spin Fe^{II} and closer to that observed in $(NBu_4)[FeCr(ox)_3]$ than to the B_{hf} reported for $Fe(ox) \cdot 2H_2O$.

The Mössbauer spectra of $[FeCp_2^*][FeRu(ox)_3]$ (Fig. 14) show the contribution of Fe in both $[FeCp_2^*]^+$ and $[FeRu(ox)_3]^-$. Between 297 and 15 K, the broad, slightly asymmetric absorption peak typical of $[FeCp_2^*]^+$ (10b) overlaps the quadrupole doublet due to $[FeRu(ox)_3]^-$. The absorption peak of $[FeCp_2^*]^+$ may be approximated by a single Lorentzian with estimated $\delta = 0.40$ and 0.52 mm/s,

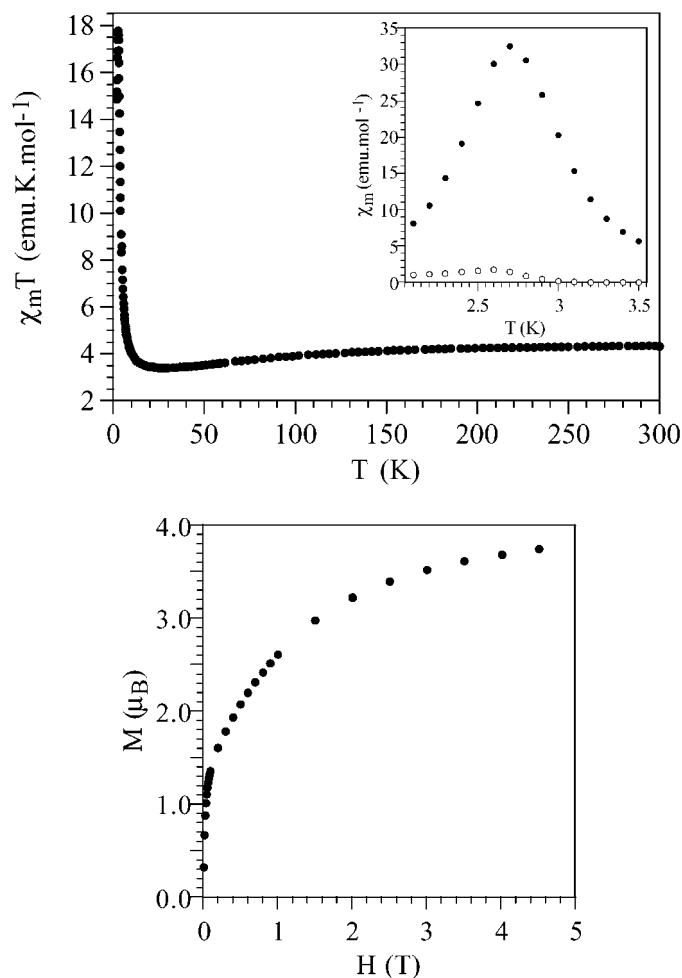at 297 and 15 K, respectively. These values compare well with those reported for $[FeCp_2^*]^+$ in other compounds, such as $\delta \approx 0.48$ mm/s at 78 K (19) or $\delta \approx 0.46$ mm/s at 140 K (10b).

The estimate δ and Δ for the $[FeRu(ox)_3]^-$ in the $[FeCp_2^*][FeRu(ox)_3]$ compound are identical, within experimental error, to those estimated for $[CoCp_2^*][FeRu(ox)_3]$. At 15 K the relative intensities of both the $[FeRu(ox)_3]^-$ and the $[FeCp_2^*]^+$ subspectra are similar, $\approx 48 \pm 2$ and $52 \pm 2\%$, respectively. This is consistent with equal numbers of Fe atoms in $[FeCp_2^*]^+$ and $[FeRu(ox)_3]^-$. A larger difference between these relative intensities was estimated at 297 K, which may be explained by different recoil-free fractions of Fe in the $[FeCp_2^*]^+$ and $[FeRu(ox)_3]^-$.

At 13 K the broadening of all the absorption peaks (Fig. 14) reflects the onset of magnetic ordering. In fact, at 5 K, the subspectrum of Fe in $[FeRu(ox)_3]^-$ is similar to the spectrum observed for $[CoCp_2^*][FeRu(ox)_3]$ at the same temperature, clearly showing magnetic ordering. The B_{hf} are slightly different but their directions relative to the electric
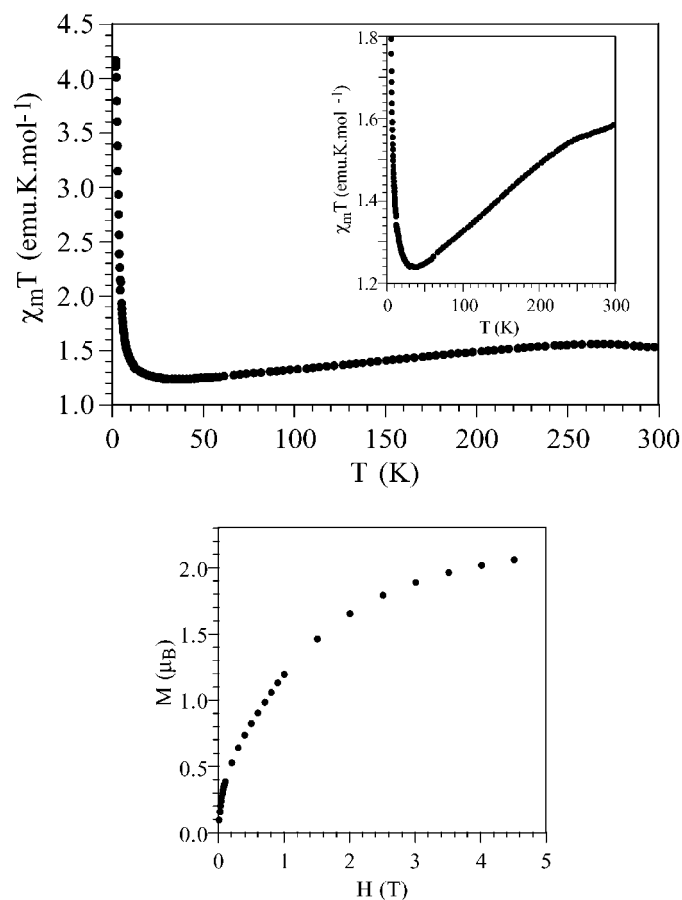

FIG. 11. (top) Plot of the $\chi_m T$ product vs T and of the ac susceptibility measurements (inset) for $[FeCp_2^*][CoRu(ox)_3]$ (**8**); (bottom) plot of the magnetization vs applied field at 2 K.

FIG. 12. (top) Plot of the $\chi_m T$ product vs T and of the ac susceptibility measurements (inset) for $[FeCp_2^*][CuRu(ox)_3]$ (**9**); (bottom) plot of the magnetization vs applied field at 2 K.

$M^{II}Ru^{III}$	C (emu K mol^{-1})	C_{SO}(emu K mol^{-1})	θ (K)	T_c (K)	$M(\mu_B)$	$M_r(\mu_B)$	H_{coer}(kOe)
MnRu	5.4	5.48	0.3	< 2	6.5	0	0.00
FeRu	4.9	4.51	7.8	13.8	4.1	2.5	2.21
CoRu	4.6	4.15	− 17.1	3.1	3.8	0	0.00
CuRu	1.7	1.55	− 1.1	< 2	2.1	0	0.00
ZnRu	1.2	1.10	− 8.3	—	1.8	—	—

Note. Parameters are experimental Curie constant C, calculated spin-only Curie constant (C_{SO}), Weiss constant (θ), critical temperature (T_c), magnetization at 50 kOe and 2 K (M), remnant magnetization at 2 K (M_r) and coercive field at 2 K (H_{coer}).

field gradient axes are the same in both compounds (Table 5). At 13 K (Fig. 14) the central absorption peak of $[FeCp_2^*]^+$ becomes less intense, since the total area of the $[FeCp_2^*]^+$ contribution is redistributed over a much wider velocity range, as in the case of $[FeCp_2^*][MCr(ox)_3]$ (M = Co, Fe) below the corresponding T_c (10b). The peak base broadens in such a way that the total contribution can no longer be approximated by a single Lorentzian. This shows that in the $[FeCp_2^*][FeRu(ox)_3]$, as in the other oxalate bimetallic compounds, the fluctuations in the electron spin of the Fe in the $[FeCp_2^*]^+$ slow down due to the polarization by the internal magnetic fields generated by the oxalate layers below T_c.

CONCLUDING REMARKS

In this article we have shown the versatility provided by the two-dimensional bimetallic oxalate complexes to construct novel magnetic materials in which the layered

bimetallic magnets $[M^{II}Ru^{III}(ox)_3]^-$ (M = Mn, Fe, Co, and Cu) are separated by diamagnetic or paramagnetic molecular cations. We have found that [FeRu] and [CoRu] derivatives are magnets, while [MnRu] and [CuRu] ones stay as paramagnets down to 2 K. This result closely resembles that found in the analogous $(NBu_4)^+$ series. In fact, the critical temperatures of this last series are 13 and 2.9 K for Fe and Co derivatives, respectively.

One of the most important aspects derived from this work concerns the nature of the Ru^{III}–M^{II} interaction. Based on the results obtained on the $(NBu_4)[M^{II}Ru^{II}(ox)_3]$ series. Oliver Kahn proposed an antiferromagnetic interaction for the Ru–Fe and Ru–Cu pairs and a ferromagnetic one for the Ru–Mn pair. It was a surprise for Olivier that these compounds did not respect the symmetry rules governing the nature of the interaction between magnetic ions. This breakdown was attributed to the ground state of the $4d$ metal ion. In fact, in octahedral environments Ru^{III} has an orbitally degenerate $^2T_2$ ground state with a strong spin–orbit
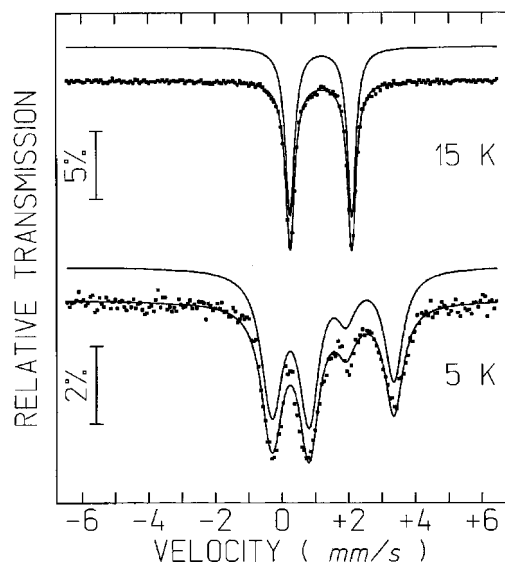

FIG. 13. Mössbauer spectra of $[CoCp_2^*][FeRu(ox)_3]$. The lines over the experimental points are the calculated functions.

Compound	T	δ	Δ, Δ'	η	B_{hf}	θ	ϕ
(2)	297	1.14	1.27				
	14	1.29	1.88				
	5	1.28	− 1.51	0.60	9.2	90°	0°
(7)	297	1.16	1.27				
	15	1.28	1.90				
	5	1.29	− 1.71	0.35	8.6	90°	0°

Note. The parameters are δ (mm/s), isomer shift relative to metallic α-Fe at 295 K; Δ (mm/s), quadrupole splitting in the paramagnetic state; $\Delta' = eQV_{zz}/2$ (mm/s), quadrupole interaction in the magnetically ordered state; B_{hf} (T), magnetic hyperfine field; and θ and ϕ, angles between B_{hf} and the main axis, V_{zz}, of the electric field gradient and between B_{hf} and V_{xx}. Estimated error are ≤ 0.02 mm/s for δ, Δ, Δ' and < 0.2 T for B_{hf}. Values of θ, ϕ, and η, kept constant during the fitting procedure, are those corresponding to the best final adjustments.

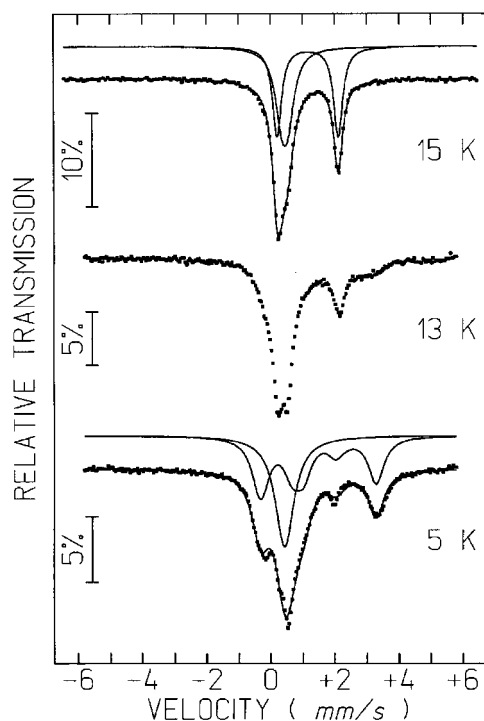**FIG. 14.** Mössbauer spectra of $[FeCp_2^*][FeRu(ox)_3]$. The lines over the experimental points are the calculated functions corresponding to the sum of the contributions of $[FeCp_2^*]^+$, single broad peak, and $[FeRu(ox)_3]^-$ similar to the spectra of $[CoCp_2^*][FeRu(ox)_3]$ at the same temperatures. Individual contributions are shown slightly shifted for clarity. At 13 K only the experimental points are plotted in order to show the onset of magnetic ordering of the Fe atoms in $[FeRu(ox)_3]^-$.

A second aspect that shows the versatility of this kind of hybrid compounds in magnetism concerns the possibility of changing the chemical composition of the extended magnetic network. Thus, by making small changes in this inorganic sublattice, the physical properties of the resulting solid solution can be fine tuned (20). Since with chromium (III) the $M^{II}Cr^{III}$ pairwise interactions are ferromagnetic while with iron (III) the $M^{II}Fe^{III}$ interactions are antiferromagnetic, a solid solution of $M^{II}(Cr^{III}Fe^{III})$ enables the study of the effect of competing interactions on the magnetic properties, Importantly, a spain glass behavior accompanied by a huge increase in the coercive fields of these magnets is then obtained. The hysteretic behavior can be easily tuned with altering the chemical composition of the material. For example, values as high as 16.7 kOe (1.67 T) have been reached with the compound $[CoCp_2^*][Fe^{II}(Cr_{0.5}^{III}Fe_{0.5}^{III})(ox)_3]$. A similar procedure has made it possible to prepare solid solutions incorporating the Ru^{III} ion into the magnetic layer (21). In this case coercive fields as high as 2.2 T have been obtained by preparing a material of composition $[CoCp_2^*]$ $[Fe^{II}(Ru_{0.5}^{III}Fe_{0.5}^{III})(ox)_3]$.

A final point worth underlining in the context of the solid state chemistry concerns the metallic composition of all these organometallic–inorganic hybrid compounds. We note that they are formed by trivalent and divalent transition metal ions in a ratio 2:1, which exactly corresponds to the stoichiometry of mixed metal oxides with spinel structure. Such a feature is being exploited by our group in preparing by thermal decomposition of these complexes novel metal oxides with precise chemical composition and particle size.

REFERENCES

1. K. Awaga, E. Coronado, and M. Drillon, *Mat. Res. Bull.* 52 (2000).
2. R. Pellaux, H. W. Schamalle, R. Huber, P. Fisher, T. Hauss, B. Ouladdiaf, and S. Decurtins, *Inorg. Chem.* **36,** 2301 (1997).
3. (a) Z. J. Zhong, N. Matsumoto, H. Okawa, and S. Kida, *Chem. Lett.* 87 (1990); (b) M. Ohba, H. Tamaki, N. Matsumoto, H. Okawa, and S. Kida, *Chem. Lett.* 1157 (1991); (c) S. Decurtins, R. Pellaux, A. Hauser, and M. E. von Arx, *in* 'Magnetism: A Supramoleclar Function" (O. Kahn, Ed.), NATO ASI Series, Vol. C484, pp. 487–508. Kluwer Academic, Dordrecht, 1996; (d) P. Day, *in* "Magnetism: A Supramolecular Function" (O. Kahn, Ed.), NATO ASI Series, Vol. C484, pp. 467–486. Kluwer Academic, Dordrecht, 1996.

coupling, while the $3d$ metals Cr^{III} and Fe^{III} have $^4A_2$ and $^6A_1$ ground states in the weak-field confirguration provided by the oxalate ligand. The results reported in the present work can help to clarify this unexpected situations. In fact, a careful analysis of our results has allowed us to propose that in all the compounds the Ru^{III}–M^{II} interaction is ferromagnetic, a situation that closely resembles that encountered in the Cr^{III}–M^{II} oxalate pairs. In fact, in both Cr^{III} and Ru^{III} the unpaired electrons are located on t_{2g}-type magnetic orbitals; in principle, and neglecting other effects such as the orbital degeneracy and the spin–orbit coupling of Ru^{III}, one can expect to observe magnetic interactions of the same type in both cases, as several of the exchange pathways are common. What can be very different is the magnitude of the interaction as it depends on the weighted sum of the various contributions involving pairs of magnetic orbitals and, while Cr^{III} has three unpaired electron in the t_{2g} orbitals, Ru^{III} has only one. Such a difference may explain the reduced critical temperatures of the Ru^{III} series as compared with those of the Cr^{III} series, since these critical temperatures depends on the magnitude of the exchange interactions (see Table 3).

4. H. Tamaki, Z. J. Zhong, N. Matsumoto, S. Kida, M. Koikawa, N. Achiwa, Y. Hashimoto, and H. Okawa, *J. Am. Chem. Soc.* **114,** 6974 (1992).

5. (a) H. Tamaki, M. Mitsumi, N. Nakamura, N. Matsumoto, S. Kida, H. Okawa, and S. Iijima, *Chem. Lett.* 1975 (1992); (b) H. Okawa, N. Matsumoto, H. Tamaki, and M. Ohba, *Mol. Cryst. Liq. Cryst.* **233,** 257 (1993).

6. (a) C. Mathonière, S. G. Carling, D. Yusheng, and P. Day, *J. Chem. Soc. Chem. Commun.* 1551 (1994); (b) C. Mathonière, J. Nutall, S. G. Carling, and P. Day, *Inorg. Chem.* **35,** 1201 (1996).

7. (a) S. Decurtins, H. W. Schmalle, P. Schneuwly, and H. R. Oswald, *Inorg. Chem.* **32,** 1888 (1993); (b) S. Decurtins, H. W. Schmalle, P. Schneuwly, J. Ensling, and P. Gütlich, *J. Am. Chem. Soc.* **116,** 9521 (1994).

8. E. Coronado, J. R. Galán-Mascarós, C. J. Gómez-García and J. M. Martínez-Agudo, *Inorg. Chem.* **40,** 113 (2001), doi: 10.1021/ic0008870.

9. (a) E. Coronado, M. Clemente-León, J. R. Galán-Mascarós, C. Giménez-Saiz, C. J. Gómez-García, and E. Martínez-Ferrero, *J. Chem. Soc. Dalton Trans.* 3955 (2000); (b) E. Coronado, J. R. Galán-Mascarós, and C. J. Gómez-García-García, *Mol. Synth. Metals* **102,** 1459 (1999); (c) M. Clemente-León, E. Coronado, J. R. Galán-Mascarós, C. Giménez-Saiz, C. J. Gómez-García, C. Rovira, and V. N. Lauhkin, *Synth. Metals* **103,** 2339 (1999).

10. (a) M. Clemente-León, E. Coronado, J. R. Galán-Mascarós, and C. J. Gómez-García, *Chem. Commun.* 1727 (1997); (b) E. Coronado, J. R. Galán-Mascarós, C. J. Gómez-García, J. Ensling, and P. Gütlich, *Chem. Eur. J.* **6,** 552 (2000).

11. E. Coronado, J.R. Galán-Mascarós, C. J. Gómez-García, and R. Burriel, *J. Magn. Magn. Mater.* **196–197,** 558 (1999).

12. E. Coronado, J. R. Galán-Mascarós, C. J. Gómez-García, and V. Laukin, *Nature* **408,** 447 (2000).

13. E. Coronado, J. R. Galan-Mascaros, and C. J. Gómez-García, *Mol. Cryst. Liq. Cryst.* **334,** 679 (1999).

14. S. Bernard, P. Yu, T. Coradin, E. Riviere, K. Nakatani, and R. Clément, *Adv. Mater.* **9,** 981 (1997).

15. J. Larionova, B. Mombelli, J. Sanchiz, and O. Kahn, *Inorg. Chem.* **37,** 679 (1998).

16. N. S. Ovanesyan, G. V. Shilov, L. O. Atovmyan, R. N. Lyubovskaya, A. A. Pyalling, and Y. G. Morosov, *Mol. Cryst. Liq. Cryst.* **273,** 175 (1995).

17. K. Ruebenbauer and T. Birchall, *Hyper. Interact.* **7,** 125 (1979).

18. W. Kündig, *Nucl. Instrum. Meth.* **48,** 219 (1967).

19. V. Gama, D. Belo, S. Rabaça, I. C. Santos, H. Alves, M. T. Duarte, J. C. Waerenborgh, and R. T. Henriques, *Eur, J. Inorg. Chem.* 2101 (2000).

20. E. Coronado, J. R. Galán-Mascarós, C. J. Gómez-García, and J. M. Martínez-Agudo, *Adv. Mater.* **11,** 558 (1999).

21. E. Coronado, J. R. Galán-Mascarós, C. J. Gómez-García, and J. M. Martínez-Agudo, *Synth. Metals*, in press.